Quantitative Evaluation of Inclusion in Deoxidation of Fe-10 Mass Pct Ni Alloy with Si, Ti, Al, Zr, and Ce

ANDREY KARASEV and HIDEAKI SUITO

The composition, size, number, and morphology of the inclusions in deoxidation of Fe-10 mass pct Ni alloys with 0.2 mass pct *M* (*M* = Si, Ti, Al, Zr, and Ce) containing mostly 60 to 130 mass ppm oxygen were studied as a function of holding time at 1873 K. It was found that the initial primary inclusions contained FeO and the FeO content decreased with an increase of deoxidation power and holding time. The mean spatial diameter of inclusions tends to increase with increasing holding time, but did not show the systematic trend with respect to the deoxidation power. The number of particle sections per unit area decreased with decreasing deoxidation power and increasing holding time. In the absence of stirring of melt, the growth rate of the mean spatial diameter of inclusions and the removal rate of particle sections per unit area decreased rapidly with increasing holding time and approached a constant after 10 minutes. The morphology of inclusions was found to be spherical, polyhedral (except Si), and irregular including cluster, and the mean spatial diameter of these inclusions increased with increasing holding time.

I. INTRODUCTION

IT has been observed in the deoxidation of steel melts with aluminum that the initial primary deoxidation products contain a large amount of FeO and then composition of primary inclusions changes with time due to the reaction between existing inclusions and dissolved Al.[1,2] During the period that the inclusions are in a fluid state, it is predicted that fluid deoxidation products have a good ability to coalesce and are rapidly removed, according to Stokes' law.[3] For this reason, it follows that the formation of FeO-containing initial inclusions has a great influence on the elimination of the inclusions from the melt under a certain turbulent flow condition. This is due to the fact that solid inclusions cannot coalesce easily in the same way as liquid inclusions are apt to do.

A considerable number of investigations have been carried out concerning the number and size of primary deoxidation products. However, there are very few systematic studies on the inclusion-coarsening characteristics for different deoxidants. Ueshima *et al.*[4] studied the time dependence of the number and size of the initial primary inclusions by adding various deoxidant elements to a low carbon steel melt. As a result, they observed that the number of inclusions in the sample obtained 30 seconds after addition increased with increasing deoxidation power of Ti < Al < Zr < Y < Hf < Ce, and the mean diameter of oxides tended to decrease in this order. However, they did not mention the formation of FeO-containing oxide inclusions.

If it is possible to disperse fine particles by introducing the primary deoxidation product into a liquid steel, a considerable influence on the mechanical properties of solid steel will be apparent through the grain-coarsening characteristics due to the pinning effect on the austenite grain boundaries, the ability to nucleate acicular ferrite, and so on.[5] In order to introduce fine primary inclusions into liquid steel uniformly, the fundamental problems such as coalescence and separation of inclusions have to be solved.

Under the aforementioned background, this study attempted to examine the nature of coagulation ability for different deoxidation products in a liquid Fe-10 mass pct Ni alloy, which was deoxidized at 1873 K with an Fe-50 mass pct *M*(*M* = Si, Ti, Al, Zr, and Ce) alloy. The inclusion characteristics such as number, size, composition, and morphology were observed as a function of holding time.

II. EXPERIMENTAL

A. *Procedure*

Deoxidation experiments were carried out in a $LaCrO_3$ resistance furnace. A charge was prepared by mixing high-purity electrolytic iron (99.99 mass pct) and globular nickel (99.97 mass pct) to obtain an overall composition of Fe-10 mass pct Ni. Iron-50 mass pct *M* (*M* = Si, Ti, Al, Zr, and Ce) alloys, which were prepared by premelting in an arc furnace, were used as a deoxidant. High-purity alumina crucible was used for the Si, Ti, and Al deoxidation, and ZrO_2-11 mol pct CaO and magnesia crucibles were used for the Zr and Ce deoxidation, respectively. The sample (100 g) was heated to 1873 K at a rate of 55 K/min for the Si, Ti, and Al deoxidation and 35 K/min for the Zr and Ce deoxidation under an argon-7 vol pct hydrogen atmosphere. Then, the melt was held for 30 minutes at 1873 K and was stirred for 2 to 3 minutes by use of an Al_2O_3 rod for the Si, Ti, and Al deoxidation and an MgO rod for the Zr and Ce deoxidation. Then, the melt was sampled by using a quartz tube for the analysis of initial oxygen content. An appropriate amount of an Fe-50 mass pct *M* alloy, which corresponded to the amount of 0.2 mass pct *M* of the sample weight, was added and immediately the melt was stirred for 20 seconds for homogenization. The sample was kept for 1, 3, or 5, and 10 (20 for the Ce deoxidation) minutes at 1873 K and then quenched in water.

ANDREY KARASEV, Graduate Student, Department of Metallurgy, and HIDEAKI SUITO, Professor, Institute for Advanced Materials Processing, are with Tohoku University, Sendai 980-8577, Japan.

Manuscript submitted July 13, 1998.

Table I. Solvent and Electrolyte Used for Dissolution of Metal Sample

Element *M*	Dissolution for Quantitative Analysis		Extraction for Observation of Particles	
	Chemical Solvent (Total *M*)	Electrolyte (Insoluble *M*)	Chemical Solvent	Electrolyte
Si	HCl-HNO_3	10 pct AA	14 wt/vol. pct iodine-methanol	4 pct MS
Ti	HCl-HNO_3-H_2SO_4	4 pct MS	14 wt/vol. pct iodine-methanol	4 pct MS
Al	HCl-HNO_3	4 pct MS	14 wt/vol. pct iodine-methanol	10 pct AA
Zr	HNO_3	4 pct MS	14 wt/vol. pct iodine-methanol	4 pct MS
Ce	HCl-HNO_3	2 pct TEA + Ba	—	2 pct TEA + Ba

10 pct AA: 10 pct acetylacetone-1 pct tetramethylammonium chloride-methanol.
4 pct MS: 4 pct methyl salicylate-1 pct salicylic acid-1 pct tetramethylammonium chloride-methanol.
2 pct TEA + Ba: 2 pct triethanol amine-1 pct tetramethylammonium chloride-methanol-(0.1 to 0.2 pct) Ba.

B. *Chemical Analysis*

All quenched ingots were cut vertically in the center. One slice of each specimen was polished with SiO_2 powder (0.06 μm) for the metallographic observation, which included light microscopy (LM), scanning electron microscopy (SEM), and electron probe microanalysis (EPMA). Metallographic study was carried out for three zones: top—1 mm below the top surface, middle—in the center, and bottom—1 mm above the bottom of the sliced specimen. Other slices were used for the chemical analysis of total and insoluble *M*, the oxygen analysis, and the extraction of inclusions in each zone of the specimen.

For the determination of total *M*, a metal sample (0.2 g) was dissolved with the solvent given in Table I. A solution was used for the analysis of total *M* by inductively coupled plasma (ICP) emission spectrometry. For the chemical analysis of insoluble *M* and Fe, a metal sample (0.3 to 0.5 g) was dissolved with 10 pct AA for SiO_2, 4 pct MS for Ti_2O_3, Al_2O_3, and ZrO_2, and 2 pct TEA for Ce_2O_3 by using an electrolytic extraction method. The compositions of electrolyte are also given in Table I. After filtration, the residue was analyzed for insoluble *M* by using ICP emission spectrometry.

The total composition of inclusions on the film filter was determined by chemical analysis after electrolytic extraction of the sample (0.3 to 0.5 g) in a manner similar to the analysis of insoluble *M*.

Total oxygen content in metal sample (0.3 to 0.5 g) was determined by inert gas fusion infrared absorptiometry using an oxygen analyzer. The details are given elsewhere.[6]

C. *Observation of Inclusions*

The particles in a polished cross section and those on the film filter after extraction were observed for the metallographic investigation of inclusion number, size, composition, and morphology. The former and the latter denote the cross-sectional method and the extraction method, respectively, hereinafter. The agglomerated deoxidation products in a cross section of the specimen were observed by using LM with a magnification of 500 or 1000. Microphotographs were taken for 24 to 36 different parts at each zone (top, middle, and bottom) of the cross section, and the number, size, and morphology of particle sections were observed by using SEM and EPMA with a magnification of 1000 or 2000. The observed area of each zone was 0.08 to 0.49 mm^2 for the Si, Ti, and Al deoxidation and 0.06 to 0.15 mm^2 for the Zr and Ce deoxidation. Total number of observed inclusions of each zone was 45 to 120 for the Si, Ti, and Al deoxidation and 80 to 270 for the Zr and Ce deoxidation.

The chemical extraction of inclusions was done for the observation of particles on the film filter in the case of an Fe-10 mass pct Ni-M (M = Si, Ti, Al, and Zr) alloy according to the method given in Table I. Metal sample was dissolved with 14 wt/vol. pct I_2-methanol under ultrasonic vibration. The amount of dissolved metal was 0.2 g. Electrolytic extraction method with 2 pct TEA containing Ba was used for the dissolution of an Fe-10 mass pct Ni-Ce alloy. The amount of dissolved metal was 0.1 g. The membrane filter with an open pore size of 0.1 μm was used for the filtration of the solution. Then, the extracted particles on the film filter were coated with carbon. Microphotographs of 6 to 8 were taken for the inclusion observation on the film filter, and the inclusion characteristics were observed by using SEM and EPMA with a magnification of 1000, 2000, 5000, and 10,000. The observed area was (1.53 to 6.78) $\times 10^{-3}$ pct of the total area of the film filter. Total number of observed inclusions on the film filter of each zone was 100 to 550 for the Si, Ti, and Al deoxidation and 200 to 700 for the Zr and Ce deoxidation. The size of particles was estimated as equivalent-area diameter by using a semiautomatic image analyzer.

III. RESULTS AND DISCUSSION

A. *Thermodynamic Considerations of Deoxidation Equilibrium*

The contents of initial ($O_{initial}$) and total (O_{total}) oxygen obtained from oxygen analysis and those of total *M* (M_{total}), insoluble *M* (M_{insol}), Al (Al_{insol}), and Fe (Fe_{insol}) obtained from chemical analysis are summarized in Table II for different deoxidants, holding time, and zone (top, middle, and bottom) of the specimen. It is to be noted that insoluble Al was observed, since an alumina crucible was used for the Si and Ti deoxidation.

The analyzed values for the soluble oxygen content ($O_{total} - O_{insol}$) are plotted against those for the content of soluble deoxidant element (M_{sol}) in Figure 1 for the Si, Ti, and Al deoxidation. The contents of insoluble oxygen (O_{insol}) were estimated from the contents of insoluble *M*, Al, and Fe obtained from chemical analysis by considering the oxides as SiO_2, Ti_2O_3, Al_2O_3, and FeO. The thermodynamic equilibrium lines were calculated at 1873 K from the equilibrium constants given in Table III, coupled with the respective interaction coefficients given in Table IV, under the assumption that the activity of M_nO_m, $a_{M_nO_m}$, is unity. The results for the Fe-10 mass pct Ni-M (M = Ti, Al)-O

Table II. The Contents of Total O, *M*, and Al and Those of Insoluble *M*, Al, and Fe as a Function of Holding Time for Different Deoxidants

Deoxidant *M*	Crucible	Time (s)	$O_{initial}$ (Mass Ppm)	Zone	O_{total}	M_{total}	Al_{total}	M_{insol}	Al_{insol}	Fe_{insol}
					(Mass Ppm)					
Si	Al_2O_3	80	119	t	89.8 to 94.2	2070	6.6	19.9	6.6	51.0
				m	86.5 to 91.4	2090	4.4	16.6	4.4	39.1
				b	93.2 to 94.6	2070	5.3	19.4	5.3	48.9
		620	104	t	87.4	2140	9.1	34.7	9.1	35.0
				m	107 to 118	NA	NA	NA	NA	NA
				b	96.3 to 102	2120	14.6	32.7	14.6	31.4
Ti	Al_2O_3	83	133	t	111	1990	46.1	208	3.6	30.2
				m	120	1970	31.4	198	4.2	27.9
				b	117	2010	31.9	203	3.4	25.4
		208	76.6	t	68.3	2030	64.0	112	4.5	6.3
				m	66.4	1970	71.7	120	4.5	6.1
				b	72.1	NA	NA	NA	NA	NA
		610	271	t	106	1530	48.9	191	6.2	5.4
				m	98.5	1580	14.3	180	6.5	4.4
				b	57.2	1590	6.2	120	2.4	2.9
Al	Al_2O_3	106	93.8	t	79.3	1840	—	80.4	—	12.7
				m	73.9 to 75.4	1890	—	78.3	—	10.7
				b	78.5	1820	—	77.1	—	7.1
		310	61.4	t	53.4 to 60.0	2070	—	52.2	—	6.4
				m	53.8 to 54.6	2090	—	49.5	—	5.2
				b	52.4 to 57.9	2090	—	54.8	—	4.9
		600	72.7	t	45.1 to 51.6	1530	—	45.7	—	4.6
				m	49.8 to 51.0	1490	—	53.7	—	4.2
				b	65.6	1520	—	60.4	—	4.6
Zr	ZrO_2	90	102	t	132 to 136	1630	—	370	—	0.4
				m	144	1470	—	389	—	13.8
				b	128	1490	—	334	—	11.5
		610	85.6	t	131 to 133	616	—	228	—	1.6
				m	161	773	—	420	—	1.8
				b	145	991	—	374	—	1.6
Ce	MgO	120	76.6	t	147	1780	—	845	—	25.9
				m	144	1890	—	812	—	38.5
				b	145	1730	—	780	—	26.8
		600	100	t	139	1210	—	719	—	4.4
				m	159	1050	—	842	—	4.3
				b	125	1160	—	761	—	1.1
		1220	109	t	131	860	—	698	—	0.3
				m	134 to 135	791	—	755	—	0.5
				b	136	814	—	726	—	0.2

t—top, m—middle, b—bottom, and NA—not analyzed.

system are indicated by thick solid lines in Figure 1, together with the thin solid lines for the Fe-M (M = Ti, Al)-O system for comparison. It can be seen that in the case of the Ti and Al deoxidation, the experimental data points fall roughly on the equilibrium line, although the data points scatter to a considerable degree. In the Fe-10 mass pct Ni alloy, the equilibrium oxygen level for a given Al level seems to be slightly higher than that for a given Ti level. This trend is different in an Fe melt. For the Si deoxidation, however, a large amount of FeO and Al_2O_3 was observed, as will be described in Section III–D. This results in the deviation from the equilibrium line of $a\ SiO_2 = 1$, as shown in the upper diagram of Figure 1. The activity of SiO_2 in the 54 pct FeO-9 pct Al_2O_3-37 pct SiO_2 slag (mass content in pct), whose composition was estimated from the contents of insoluble Fe, Al, and Si, was obtained as 0.39 using a regular solution model.[19] The experimental data fall slightly below the calculated line of $a\ SiO_2 = 0.39$, which is indicated by a thin broken line.

Figure 2 shows a similar plot to Figure 1 for the Zr and Ce deoxidation. The thin solid line was calculated from the equilibrium constant obtained by Inoue and Suito,[12] and the thick solid lines for the Zr and Ce deoxidation equilibria were calculated from the equilibrium constants and the interaction coefficients given in Tables III and IV, respectively. The reason for the positive deviation from the calculated lines is not certain, whether it is due to the uncertainty of the thermodynamic values used in the present work or due to the nonequilibrium state under such a strong deoxidation condition. Some data points for $O_{total} - O_{insol}$ shown in Figures 1 and 2 are less than zero. This unreasonable result may be due to the inaccuracy in the determination of insoluble Fe or M content. The influence of FeO in the inclusion phase on the equilibrium will be discussed in the following section.

The content of insoluble oxygen, which was estimated from the difference between the total oxygen (O_{total}) and the equilibrium soluble oxygen (O_{eq}), is compared with those

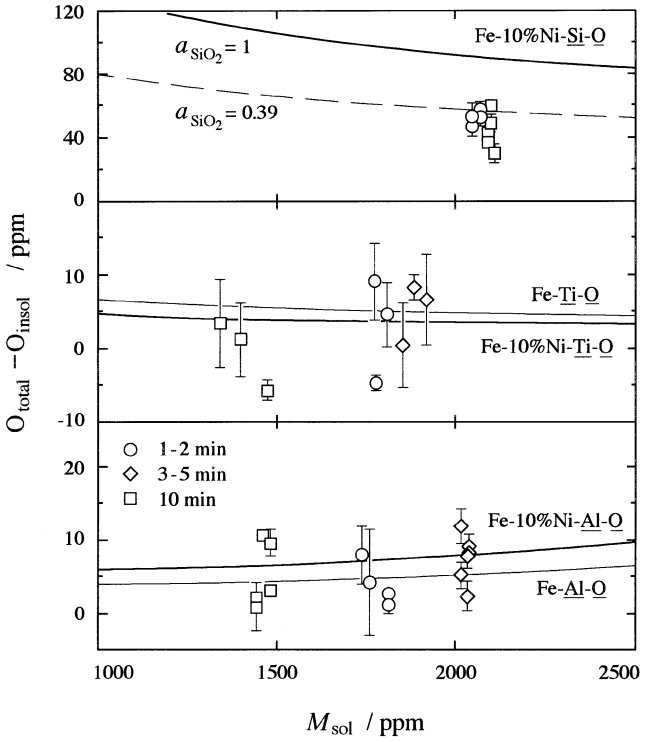

Fig. 1—Relation between soluble oxygen and soluble *M* contents in Si, Ti, and Al deoxidation at 1873 K.

Table III. Equilibrium Constants Used for the Calculation of Equilibrium Line

Reaction	log K	Reference
SiO_2 (s) = Si +2 O	11.59 − 30,400/*T*	7, 8
Ti_2O_3 (s) = 2Ti + 3O	18.35 − 56,348/*T*	8, 9
Al_2O_3 (s) = 2Al + 3O	20.18 − 62,790/*T*	7, 8
ZrO_2 (s) = Zr + 2O	−9.87 at 1873 K	10
	11.80 − 40,750/*T*	11
	−9.83 at 1873 K	12
Ce_2O_3 (s) = 2Ce + 3O	19.60 − 68,500/*T*	13
	−17.03 at 1873 K	14

of insoluble oxygen (O_{insol}) obtained from the chemical analysis of insoluble *M*, Al, and Fe. The results for all deoxidation experiments are shown in Figure 3, indicating good correspondence between the two values.

B. *Time Dependence of Insoluble M Content*

The contents of total and insoluble *M* obtained from chemical analysis for each zone of the specimen and those of the initial *M*, which was initially added, are plotted against different deoxidants in Figure 4, in which the results for the short and long holding times are shown in the upper and lower diagrams, respectively. The content of the initial *M* for each experiment was calculated from the weight of the initial charge and the amount of added deoxidant along with the weight used for sampling for the analysis of initial oxygen. The deoxidants are plotted from Ce to Si, which is in the decreasing order of the deoxidation power. It can be seen that the contents of the removed *M* from the bulk phase increase with increasing the deoxidation power and holding time at 1873 K. The contents of the dissolved *M*,

Table IV. Interaction Coefficients Used in the Present Work

i	*j*	e_i^j	r_i^j	Reference
O	Si	−0.131	0	8
	Ti	−0.6	0.031	8
	Al	7.15 − 20,600/*T*	1.7	8
	Zr	−0.044	—	8
	Ce	−0.57	—	8
	Ni	0.006	0	8
	O	0.734 − 1750/*T*	0	8
Si	Si	0.089 + 34.5/*T*	−0.0055 + 6.5/*T*	8
	Al	0.058	—	8
	Ni	0.005	0	8
	O	−0.23	—	8
Ti	Ti	0.013	−0.001	8
	Ni	0.009	0.0005	15
	O	−1.8	—	8
Al	Al	0.011 + 63/*T*	−0.0011 + 0.17/*T*	8
	Ni	−0.0376	0.000164	16
	O	11.95 − 34,740/*T*	—	8
Zr	Zr	0.02	—	17
	O	−2.6	—	11
Ce	Ce	0.004	—	18
	O	—	—	—

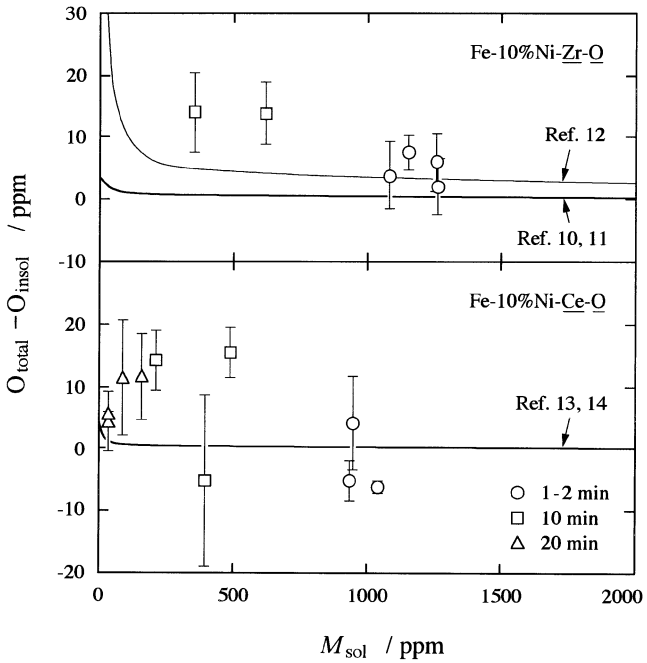

Fig. 2—Relation between soluble oxygen and soluble *M* contents in Zr and Ce deoxidation at 1873 K.

on the other hand, decrease with time, particularly for the case of Ce and Zr, which have high deoxidation power. The content of insoluble *M*, which corresponds to the content of inclusions present in the bulk metal, does not change much with increasing holding time, as compared with the contents of removed and dissolved *M*.

Two types of layers consisting of different amounts of deoxidation product, M_nO_m and FeO, were observed at the top surface of the specimen in all experiments, as shown schematically in Figure 5. The upper layer (L1) with 5 to 40 μm in thickness contained high FeO, but the content of FeO and the thickness of this layer were found to decrease

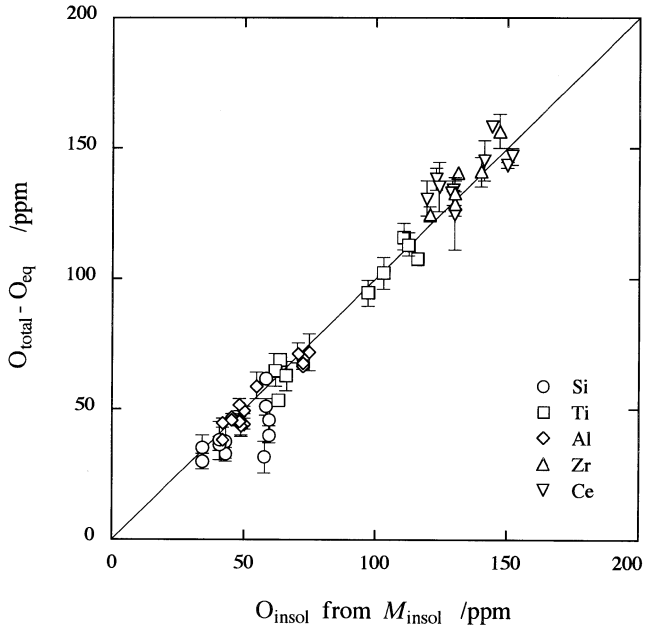

Fig. 3—Insoluble oxygen contents obtained from total oxygen and equilibrium soluble oxygen plotted against insoluble oxygen content estimated from analyzed insoluble *M*, Al, and Fe.

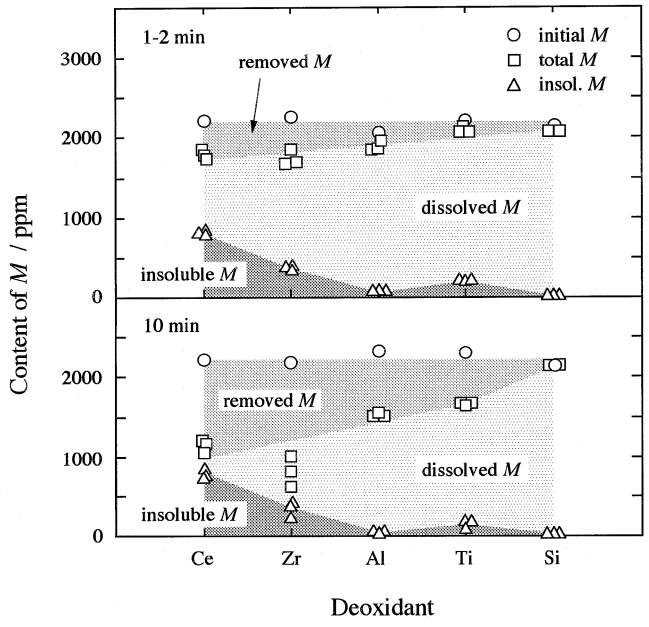

Fig. 4—Initial, total, and insoluble deoxidant, *M*, after deoxidation at 1873 K.

with increasing holding time. The lower layer (L2) with 5 to 60 μm in thickness contained deoxidation product from 15 to 25 mass pct for the Si deoxidation to 40 to 50 mass pct for the Ce deoxidation. Furthermore, the thickness and the content of M_nO_m of this layer increased with increasing holding time.

In the case of the deoxidation with Zr and Ce, the deoxidation products, which consisted of polyhedral—25 to 70 μm and needlelike—30 to 90 μm particles in cluster for the Zr and Ce deoxidation, respectively, were observed along the wall (L3) and at the bottom (L4), as illustrated schematically in Figure 5. It was found that the thickness

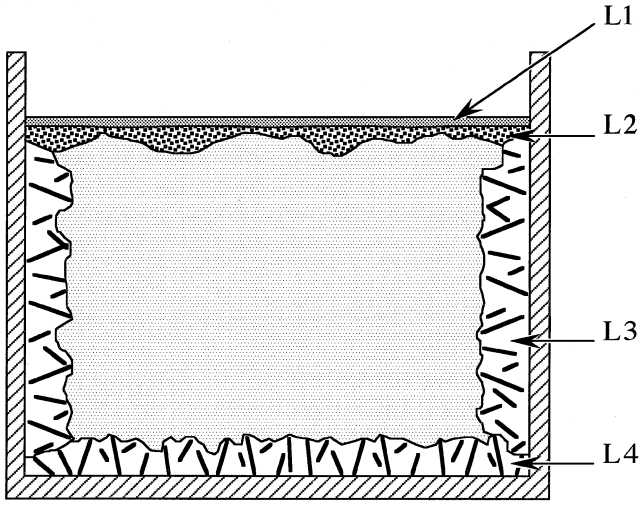

Fig. 5—Schematic illustration of layers of deoxidation products in metal sample.

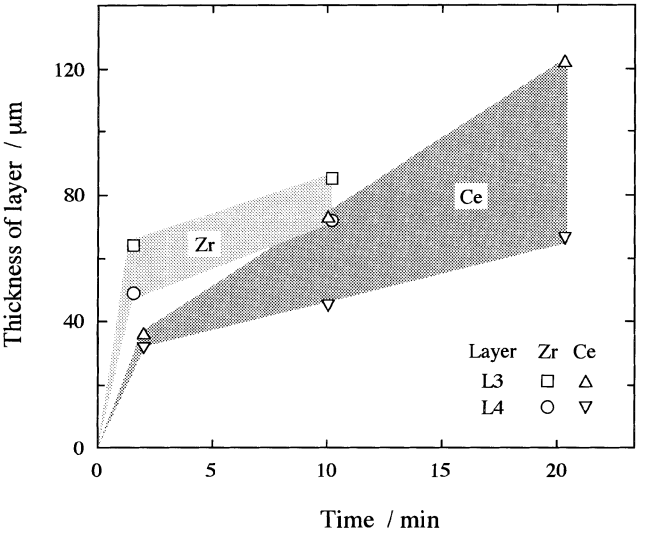

Fig. 6—Change of layer thickness with time at metal-crucible boundary in Zr and Ce deoxidation.

of layers L3 and L4 increased with increasing holding time, as shown in Figure 6, indicating that the rate of the increase decreases with time. The increase of the thickness with holding time is consistent with the behavior with respect to the removal of the deoxidation products, as shown in Figure 4. In the experiments of the deoxidation with Ce and Zr, the removal rate is considerably fast in the range from 1 to 2 to 10 minutes, whereas in the experiments of the deoxidation with Si, Ti, and Al, the removal rate is relatively slow.

C. *Number and Size of Inclusions*

The mean spatial diameter of inclusions, $\overline{d}_V$, and the number of particle sections per unit area, N_A, are shown in Figure 7 as a function of holding time. The inclusion size and the inclusion number were obtained from the extraction and the cross-sectional methods, respectively, by using a magnification of 1000. The $\overline{d}_V$ value was determined as the arithmetic mean diameter of particles on the film filter. The

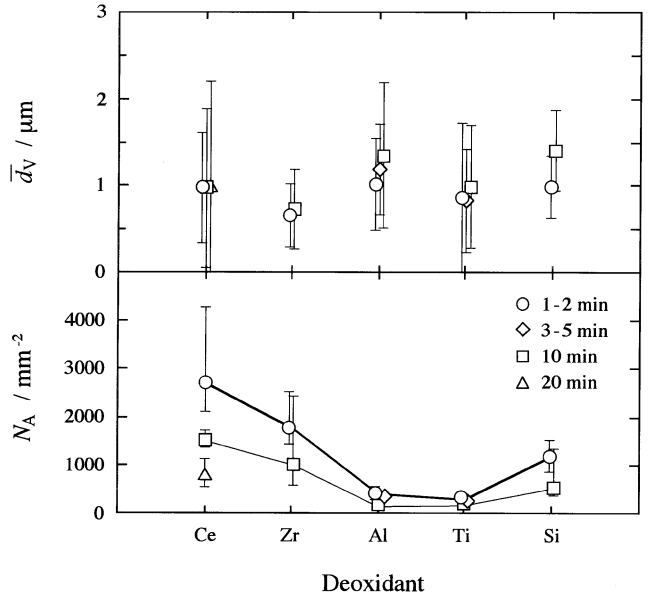

Fig. 7—Mean spatial diameter of particles, $\bar{d}_V$, and number of particle sections per unit area, N_A.

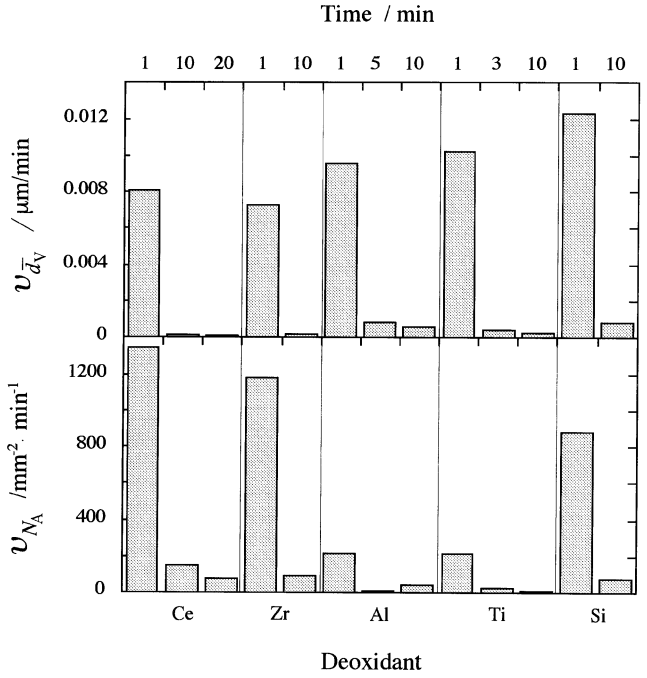

Fig. 8—Average growth rate of mean spatial diameter of inclusions, $\bar{d}_V$, and removal rate of particle sections per unit area, N_A, plotted against holding time and different deoxidants.

N_A value was obtained by n/A_{obs}, where n and A_{obs} are the number of particles and observed area in a cross section, respectively. Error bars represent the arithmetic standard deviation for the $\bar{d}_V$ values and the range of the maximum and the minimum values for the N_A values, respectively. In short time experiments, the mean spatial diameter of initial primary inclusions was almost the same for all deoxidants, and no systematic increase with respect to the deoxidation power was observed. The number of particles per unit area for the holding time of 1 to 2 minutes decreased with decreasing deoxidation power from 2700 particles/mm^2 for the Ce deoxidation to 290 to 380 particles/mm^2 for the Ti and Al deoxidation. The reason that the Si deoxidation has a different behavior can be interpreted by the high content of soluble oxygen for a given Si level after deoxidation, which results in the formation of secondary inclusions during solidification. It is seen that the N_A values for all deoxidants decrease with an increase of holding time. The results for the $\bar{d}_V$ and N_A values obtained from the size distribution by using different magnifications are discussed in detail elsewhere.[20]

The supersaturation ratio $S\{ = (a^n_M \cdot a^m_O)_{ss}/(a^n_M \cdot a^m_O)_{eq}\}$ under the present experimental conditions was estimated at 1873 K from the initial contents of M (0.2 mass pct) and O (100 mass ppm) and the equilibrium constants given in Table III, coupled with the respective interaction coefficients given in Table IV. These values in logarithmic form for the Ce, Zr, Al, Ti, and Si deoxidation were found to be 9.41, 5.25 (3.48 from Reference 12), 3.18, 2.20, and 0.08, respectively. This decreasing order is on line with the present results for the number of particle sections per unit area, except for the case of Si, but not on line with those for the mean spatial diameter of inclusions, which is shown in Figure 7. In order to explain these results based on the classical homogeneous nucleation theory, the values for the interfacial tension between the matrix and the respective deoxidation products and those for the corresponding molar volume are necessary in addition to the degree of supersaturation. Since the accurate values for the interfacial tension are not available, the decreasing order of a number of particles per unit volume, N_V $(=N_A/\bar{d}_V)$, cannot be interpreted solely by the degree of supersaturation.

The growth rate of mean spatial diameter of inclusions $(\upsilon_{\bar{d}_V})$ defined by $\Delta\bar{d}_V/\Delta\tau$, where $\Delta\bar{d}_V = \bar{d}_V(\tau_2) - \bar{d}_V(\tau_1)$ and $\Delta\tau = \tau_2 - \tau_1$, and the removal rate of particle sections per unit area (υ_{N_A}) defined by $\Delta N_A/\Delta\tau$, where $\Delta N_A = N_A(\tau_1) - N_A(\tau_2)$, are plotted against holding time (τ) for different deoxidants in Figure 8. It is seen that the growth rate of mean spatial diameter of inclusions decreases and the removal rate of particle sections per unit area increases, except for Si, with increasing deoxidation power. Furthermore, the values for $\upsilon_{\bar{d}_V}$ and υ_{N_A} decrease considerably with increasing holding time, and after 10 minutes, they approach a constant.

The number of particles per observed area on the film filter having the size for <0.4 and 0.4 to 0.9 μm and that for 1.0 to 1.9 and ≥ 2.0 μm are plotted against holding time for different deoxidants in Figures 9 and 10, respectively. As shown in Figure 9, the number of particles per observed area over short time experiments for the Ce and Zr deoxidation is greater than that for the Si, Ti, and Al deoxidation. By increasing holding time, however, the number of inclusions with this size decreases considerably for Ce_2O_3 and ZrO_2, while it does not change much for SiO_2, Ti_2O_3, and Al_2O_3.

As shown in Figure 10, the number of particles in the range of large size does not show the systematic trend with respect to the deoxidation power. The number of particles per observed area having the size of 1.0 to 1.9 μm does not change with holding time for all deoxidants, except for Ce, as shown in the upper diagram. However, the number of large size inclusions (≥ 2.0 μm) increases with holding time, except for Ti, as shown in the lower diagram. The number of inclusions in the range of large size could not

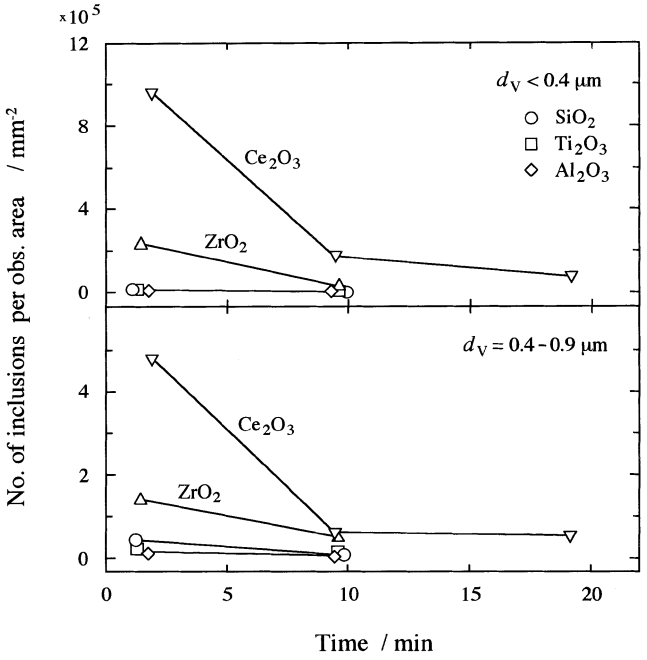

Fig. 9—Number of inclusions per observed area on film filter, having the size smaller than 1 μm.

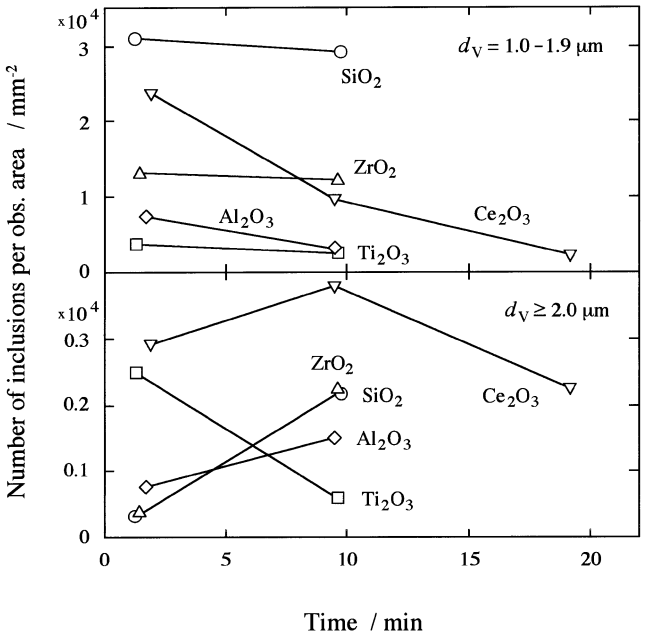

Fig. 10—Number of inclusions per observed area on film filter, having the size greater than 1 μm.

be measured accurately due to the limit of the observed area. The variation of size distribution with holding time is discussed in another article[20] in detail. Since the number of inclusions is determined by the factors related to stirring, coagulation, coalescence, and flotation, the inclusion composition seems to be of great importance.

D. *Effect of Holding Time on Composition and Morphology of Inclusions*

The composition of inclusions in different deoxidation experiments was obtained by using the analyzed contents

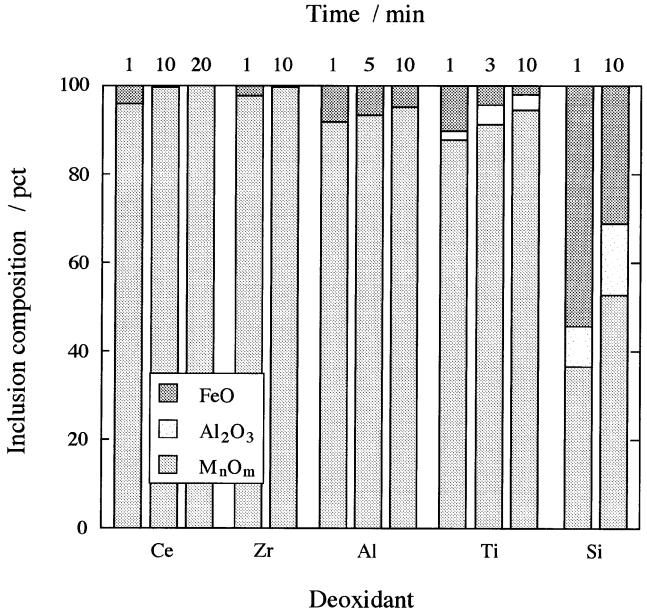

Fig. 11—Change of inclusion composition in different deoxidation experiments.

of insoluble *M*, Al, and Fe given in Table II. The results are shown in a bar graph in Figure 11. It can be seen that in short time experiments of 1 to 2 minutes holding time, the initial primary inclusions contain FeO ranging from 2 to 4 mass pct for the Zr and Ce deoxidation to 50 to 54 mass pct for the Si deoxidation. The content of FeO decreases with an increase of holding time, and for the Zr and Ce deoxidation, the inclusions composition is almost pure ZrO_2 and Ce_2O_3 after 10 minutes. For the Ti and Al deoxidation, however, inclusions contain 2 to 5 mass pct FeO even after 10 minutes. For the Si deoxidation, the FeO content decreases with holding time, but after 10 minutes, inclusions still contain a considerable amount of FeO (29 to 33 mass pct).

It has been known that in the deoxidation of molten iron by a deoxidant, the initial primary inclusions contain FeO and the FeO content decreases due to the reduction by the dissolved deoxidant element.[2] The FeO-containing inclusions may be explained by the formation of metastable phase such as FeO-M_nO_m from the supersaturated solution of liquid iron after adding a deoxidant.[21] Therefore, the formation of metastable phase depends on the degree of the critical supersaturation for the homogeneous nucleation and the degree of FeO content depends on the reducing power of deoxidant. The fact that the inclusions obtained in the Ti and Al deoxidation contain 2 to 5 mass pct FeO even after 10 minutes is probably due to the incomplete reduction of FeO present inside agglomerated particles by deoxidant in the absence of continuous stirring of melt.

The morphology of inclusions was found to be spherical, polyhedral, and irregular including clustered. The amount and the mean spatial diameter of spherical, polyhedral, and irregular inclusions obtained by the extraction-filtration method are shown in Figures 12 and 13, respectively. It can be seen from Figure 12 that in the Ti, Al, Zr, and Ce deoxidation, all types of inclusions were observed, whereas the inclusions in the Si deoxidation have no polyhedral shape due to the fact that deoxidation products contain a large

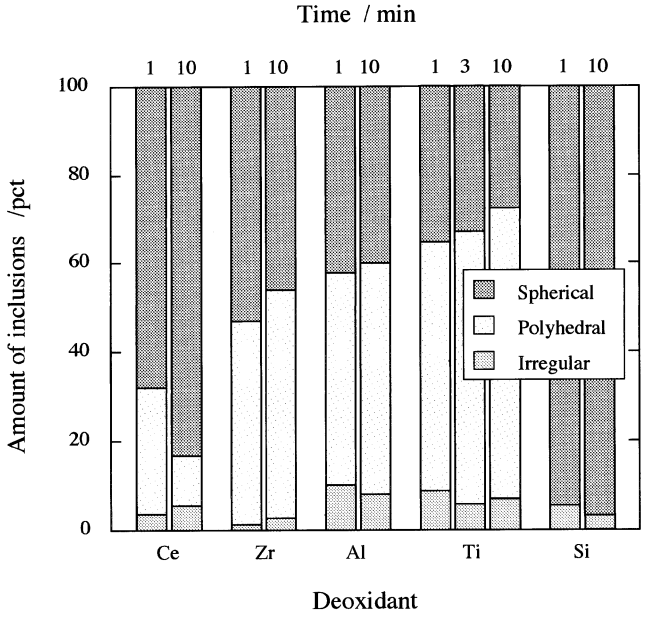

Fig. 12—Amount of spherical, polyhedral, and irregular inclusions for different deoxidation experiments.

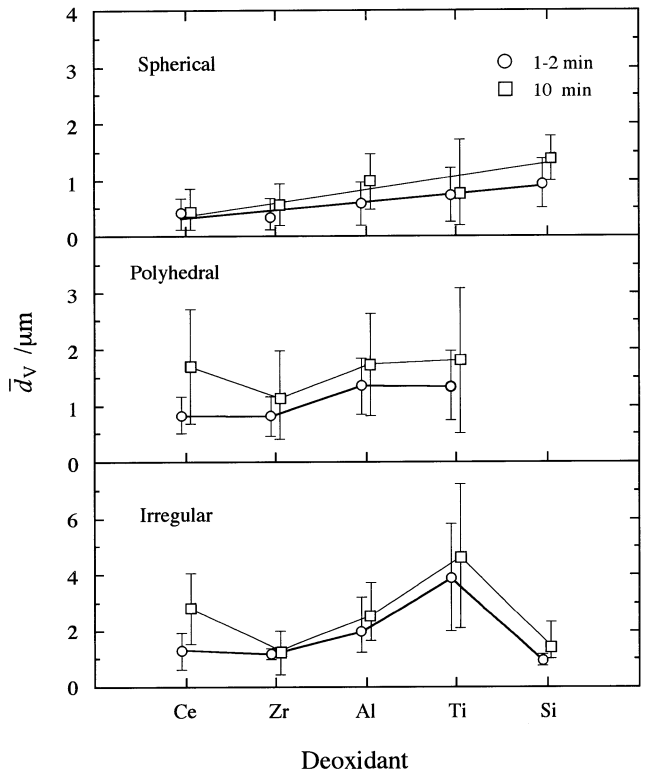

Fig. 13—Mean spatial diameter of spherical, polyhedral, and irregular inclusions for different deoxidation experiments.

amount of FeO and thus are in a fluid state at 1873 K. The amount of spherical inclusions increases and that of polyhedral inclusions decreases with increasing deoxidation power, except Si. As shown in Figure 13, the mean spatial diameter of all types of inclusions increases on the whole with holding time. The $\bar{d}_V$ values of spherical inclusion decrease with increasing the deoxidation power, but those of polyhedral and irregular inclusions do not show the systematic trend with respect to the deoxidation power. The mean spatial diameter of inclusions having different morphology increases in the order spherical (0.43 to 1.39 μm) < polyhedral (0.81 to 1.80 μm) < irregular (0.95 to 4.64 μm) for all deoxidants.

IV. CONCLUSIONS

The composition, size, number, and morphology of the primary inclusions in the deoxidation of Fe-10 mass pct Ni alloys with 0.2 mass pct M (M = Si, Ti, Al, Zr, and Ce) containing mostly 60 to 130 mass ppm oxygen were studied at 1873 K as a function of holding time. The following conclusions were obtained.

1. In all deoxidation experiments without continuous stirring, the initial primary deoxidation products contained FeO and the content of FeO decreased with increasing the deoxidation power and holding time.
2. The contents of insoluble oxygen calculated from the chemical analysis of insoluble M, Al, and Fe agreed well with those of insoluble oxygen, which were obtained by the difference between the contents of total oxygen and those from equilibrium oxygen.
3. The mean spatial diameter of inclusions tended to increase with increasing holding time, but did not show the systematic trend with respect to the deoxidation power. The number of particle sections per unit area decreased with decreasing deoxidation power and with increasing holding time. In the absence of stirring of melt, the growth rate of mean spatial diameter of inclusions and the removal rate of particle sections per unit area decreased rapidly with holding time and approached a constant after 10 minutes.
4. The morphology of inclusions was found to be spherical, polyhedral (except Si), and irregular including clustered. The mean spatial diameter of these inclusions increased with an increase in holding time.

REFERENCES

1. P.E. Wandby and W.J.M. Salter: *J. Iron Steel Inst.*, 1971, vol. 211, pp. 518-23.
2. H. Fredriksson and O. Hammar: *Metall. Trans. B*, 1980, vol. 11B, pp. 383-408.
3. N.F. Grevillius: *Jernkont. Ann.*, 1969, vol. 153, pp. 547-72.
4. Y. Ueshima, H. Yuyama, S. Mizoguchi, and H. Kajioka: *Tetsu-to-Hagané*, 1989, vol. 75, pp. 501-08.
5. O. Grong and D.K. Matlock: *Int. Metall Rev.*, 1986, vol. 31 (1), pp. 27-48.
6. R. Inoue and H. Suito: *Mater. Trans. Jpn. Inst. Met.*, 1991, vol. 32, pp. 1164-69.
7. J.F. Elliott, M. Gleiser, and V. Ramakrishna: *Thermochemistry for Steelmaking*, Addison-Wesley Publishing Co., Reading, MA, 1963, vol. 2.
8. G.K. Sigworth and J.F. Elliott: *Met. Sci.*, 1974, vol. 8 (9), pp. 298-310.
9. I. Barin: *Thermochemical Data of Pure Substances*, VCH, Weinheim, 1989.
10. Z. Buzek: *Chemical Metallurgy of Iron and Steel*, ISI, Philadelphia, PA, 1971, p. 173.
11. A. Jacquemot, C. Gatellier, and M. Olette: *IRSID Report*, 1974, Apr., Report No. 109.
12. R. Inoue and H. Suito: *CAMP-ISIJ*, 1997, vol. 10, p. 216.
13. A. Jacquemot and C. Gatellier: *IRSID Report PCM*, 1973, Aug., Report No. 63.

14. D. Janke and W.A. Fischer: *Arch. Eisenhüttenwes.*, 1978, vol. 49, pp. 425-30.
15. H. Wada and R.D. Pehlke: *Metall. Trans. B*, 1977, vol. 8B, pp. 443-50.
16. S.W. Cho and H. Suito: *Steel Res.*, 1995, No. 6, pp. 237-43.
17. Z. Buzek and A. Hutla: *Freiberger Forschüng, H.-B.*, 1969, vol. 117, pp. 59-73.
18. A. Ejima, K. Suzuki, N. Harada, and K. Sanbongi: *Trans. Iron Steel Inst. Jpn.*, 1977, vol. 17, pp. 349-58.
19. V.A. Grigorian, A.J. Stomahin, A.G. Ponomarenko, L.N. Belyanchikov, Yu.I. Utochkin, G.I. Kotelnikov, and O.I. Ostrovsky: *Physical-Chemical Calculation of Electric Steelmaking Processes*, Metallurgizdat, Moscow, 1989.
20. A.V. Karasev and H. Suito: *Metall. Mater. Trans. B*, 1999, vol. 30B, pp. 259-70.
21. M.L. Turpin and J.F. Elliott: *J. Iron Steel Inst.*, 1966, vol. 204, pp. 217-25.